On the Setup of a Test Bench for Predicting Laminar-to-Turbulent Transition on a Flat Plate

Pascal Bader and Wolfgang Sanz

Institute for Thermal Turbomachinery and Machine Dynamics, Graz University of Technology, Inffeldgasse 25/A, Graz 8010, Austria

Abstract: At turbomachinery relevant flow conditions the boundary layers are often transitional with laminar-to-turbulent transition occurring. The characteristics of the main flow can depend highly on the state of the boundary layer. Therefore it can be vitally important for the designer to understand the process of laminar-to-turbulent transition and to determine the position and length of the transitional region. In this paper the flow over a flat plate is experimentally studied in order to investigate and better understand transitional flow. Preston tube measurements as well as a thermographic camera system were performed for two different inlet velocities in order to determine the position of the transitional zone. The results of the experiment are compared to numerical flow solutions using a common transition model to determine its capability. The simulation has been performed with the two commercial codes CFX® and Fluent® by Ansys® and an in-house code called LINARS. As a result of this study, a better understanding of the experimental and numerical methods for determining transition shall be given.

Key words: Boundary layer transition, computational fluid dynamics, Preston tube, thermographic camera, flat plate boundary layers.

Nomenclature

a	Decay exponent
c_f	Wall friction coefficient
crit	Critical value
f	Frequency
H	Hydraulic/Characteristic diameter
H	Channel height
k	Turbulence kinetic energy
K	Acceleration parameter
L	Physical integral length scale
L	Plate length
l	Pseudo-integral scale
l_m	Mixing length
mean	Mean value
Nu	Nusselt number
p	Local static pressure
p_t	Total pressure
q_{probe}/q_∞	Non-dimensional dynamic pressure
Re	Reynolds number
Tu	Turbulence intensity
u	Local streamwise velocity
u_∞	Free-stream velocity
W	Channel width
x	Streamwise coordinate
y	Distance to the wall
y^+	Dimensionless wall distance
α	Heat transfer coefficient
δ	Boundary layer thickness
δ^*	Displacement thickness
ϵ	Dissipation rate
ν	Kinematic viscosity
τ_W	Wall shear stress
τ_t	Turbulent shear stress
∞	Free-stream value
$\overline{}$	Mean value
$\widehat{}$	Fluctuation

Abbreviation

ACF	Autocorrelation function
BL	Boundary layer
CFD	Computational fluid dynamics
FFT	Fast fourier transformation
FRAPP	Fast-response aerodynamic pressure probe
ITTM	Institute for Thermal Turbomachinery and Machine Dynamics
LDV	Laser Doppler velocimetry
LE	Leading edge
PIV	Particle image velocimetry

Corresponding author: Pascal Bader, Dipl.-Ing., BSc, research assistant, research field: measurement and simulation of boundary layer behavior.

SST	Shear stress transport
TE	Trailing edge

1. Introduction

The boundary layer represents the small zone between the wall and the free stream where viscous effects are important. Due to its size, the influence of its state (laminar or turbulent) is often neglected although it can have a high impact on the flow characteristics like heat transfer or wall friction. These parameters influence the efficiency as well as the thermal stress of, for example a turbine blade.

Many parameters like free-stream velocity, acceleration, free-stream turbulence etc. have an influence, if a boundary layer is laminar or turbulent, but at the first contact of a flow with a stationary structure the boundary layer starts laminar and will become turbulent (under the right flow conditions) via a transitional area. The boundary layer passes through several stages within this transitional zone until it becomes fully turbulent [1].

It is vitally important to understand the influence of the above stated parameters on the onset and length of the transitional zone in order to influence and potentially control the state of the boundary layer.

Because of the possibility to increase efficiency, transition also plays a major role in turbomachinery flows. In such machines the efficiency of blades and stages can be improved when considering transition; thus this gives the possibility to improve the overall engine performance. In 1991, Mayle [2] published an interesting overview of the role of transition in gas turbines. He analyzed experiments performed by different research groups and showed the influence of several flow parameters on the transition process.

Additional experiments were performed in the last years by different research groups. Yip et al. [3] performed inflight measurements and predicted transition with the help of Preston tubes and analyzed the influence of the flight condition on the boundary layer around an airfoil. Oyewola et al. [4, 5] showed how the flow in the boundary layer can be measured

with the help of hot-wire probes as well as LDV (laser-Doppler velocimetry). Another optical measurement technique has been used by Widmann et al. [6] who performed near-wall measurements with a PIV (particle image velocimetry) system. Also hot-film measurements were performed by Mukund et al. [7].

In addition to measurements, also different numerical approaches have been developed to predict the laminar-turbulent transition process. Common models, for example the $k - k_L - \omega$ [8] and the $\gamma - Re_\Theta$ [9, 10] model. For the latter model, various correlations for important model parameters have been developed [11-15].

So far, only the transition from laminar to turbulent has been described, but under certain flow conditions (like high acceleration) a reverse-transition or relaminarization from turbulent to laminar can occur. Up to now only few measurements and publications have been made in order to understand relaminarization. Therefore, a project has been launched at the ITTM (Institute for Thermal Turbomachinery and Machine Dynamics) at Graz University of Technology in order to understand the different mechanisms leading to relaminarization.

The first step of this project is to set up a test bench in order to measure transition from laminar to turbulent.

This should help to improve the understanding of transition even further and to test different measurement techniques. Another point of this measurement campaign is to acquire all data necessary for the simulation since the vital parameter of the turbulence scale is not documented in most experimental works. Some works discuss the measurement of turbulence length scales, for example Camp and Shin [16] who described in detail how to process the measured signal in order to get the necessary values. Also Axelsson et al. [17, 18], and Craft [19] discussed different length scales and measurements of turbulence intensity.

This work focuses on the set up of the test bench and will give an overview of technical considerations

which should be taken into account. Additionally measurement techniques are discussed and a special focus lies on measuring of the turbulence length scale.

Finally, several CFD codes and transition models will be compared in order to see their differences and their capabilities in predicting transition within the test bench.

2. Numerical Setup

The computational mesh models the flow region in the test bench which is described in the next section (Fig. 1b) and consists of about 13 million cells. To ensure a mesh independence of the simulation result, the y^+-value of the mesh was kept between 0.1 and 1 as recommended in Ref. [20]. The mesh consists only of the upper part of the channel and is illustrated in Fig. 1a.

The computational simulations have been performed with three different codes: ANSYS® CFX® v15.0, ANSYS® Fluent® v15.0.0 and the in-house code LINARS.

CFX® solves the Navier-Stokes equation system with first-order accuracy in areas where the gradients change sharply to prevent overshoots and undershoots to maintain robustness, and with second-order in flow regions with low variable gradients to enhance accuracy [20].

Fluent® uses the simple algorithm for the pressure-based solver. The pressure correction equation is solved with second-order accuracy and the momentum as well as the turbulence and transition equations are solved with a third-order MUSCL algorithm.

LINARS has been developed at Graz University of Technology at the ITTM [21]. The code solves the RANS (Reynolds-averaged Navier-Stokes) equations in conservative form with a fully-implicit, time-marching finite-volume method. The inviscid (Euler) fluxes are discretized with the upwind flux difference splitting method in Ref. [22]. The incompressible solutions are obtained with a pseudo-compressibility method.

For the simulation with all three codes Menter's $k - \omega$ SST turbulence model [23] was used with the $\gamma - Re_\Theta$ [12] transition model. Additionally, with Fluent® the $k - k_L - \omega$ [8] turbulence/transition model was also applied.

3. Experimental Setup

The measurements are performed in a subsonic wind tunnel located at the ITTM. The test rig is a continuously operating open-loop wind tunnel. The air is delivered by a 125 kW radial compressor with a flow rate of approximately 0.6 kg/s. The compressor delivers the air into a flow settling chamber. From this chamber the air is transported via a flow-calming section
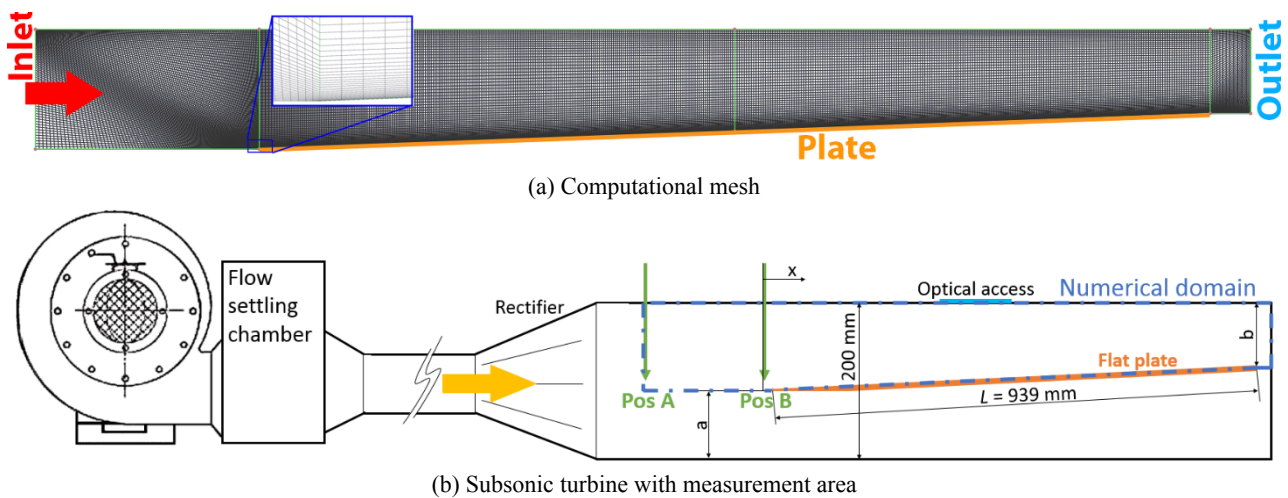

(a) Computational mesh

(b) Subsonic turbine with measurement area

Fig. 1   Illustration of the test bench and computational mesh.

formed by a diffuser with guiding vanes towards the test area. A schematic drawing of the test bench is given in Fig. 1b.

Transition measurements have been performed for two different inlet velocities: $u_{\infty,mean}$ = 5.3 m/s (low speed case) and $u_{\infty,mean}$ = 13.2 m/s (high speed case).

The plate in the channel is inclined by 2° as recommended by Coupland [24]. This should ensure that the flow is attached to the plate without leading edge separation bubbles.

In order to minimize the influence of the channel walls on the measured boundary layer some aspects have been kept in mind and will be discussed in the following.

First, the position (normal to streamwise direction) of the plate leading edge (distance a in Fig. 1b) has been chosen. One aspect here is that the plate must not be inside the boundary layer of the bottom or top wall of the channel. Therefore the approximate size of the boundary layer was estimated. The size of the boundary layer depends amongst others on the development length. It can be approximated with the Blasius solution for the laminar boundary layer:

$$\delta(x) \approx \frac{x}{\sqrt{Re_x}} \qquad (1)$$

and for the turbulent boundary layer:

$$\delta(x) \approx 0.382 \cdot \frac{x}{Re_x^{1/5}} \qquad (2)$$

where, δ is the local boundary layer thickness, x is the development length and Re_x is the Reynolds number based on x [1]. For the calculation of the Reynolds number u and v are taken at the inlet.

These two equations are illustrated in Fig. 2a which gives an example of the boundary layer growth for a specific velocity (here about 5 m/s). In this illustration of the boundary layer thickness $Re_{x,crit} = 3 \times 10^5$ is assumed for the onset of transition. According to Schlichting and Gersten [1], this is valid for "normal" longitudinal flow along a flat plate with a sharp leading edge. Additionally they state that, this critical Reynolds-number can be increased to
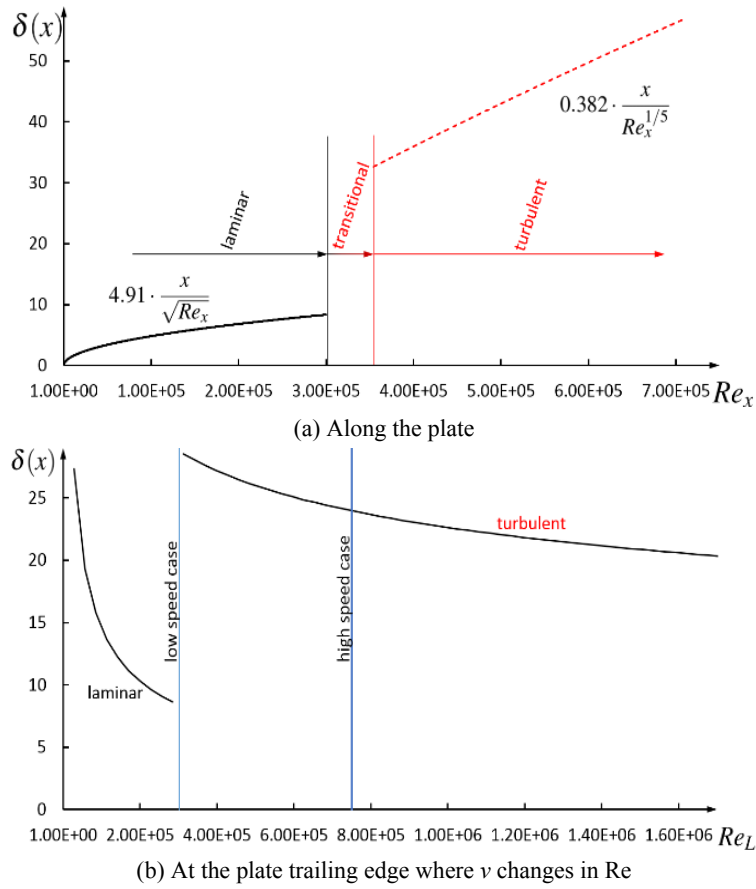
$Re_{x,crit} \approx 10^6$ by ensuring a smooth flow (low turbulence intensity).

Although it is not clear, if these transition onset criteria stated by Schlichtung and Gersten are valid for the designed test bench, it is a good start for estimating the beginning of transition. In the following, $Re_{x,crit} = 3 \times 10^5$ is assumed as the onsetlocation of the transitional zone within the test bench of the institute.

The Re_L [1] value of the bottom and top wall, respectively, can be estimated with about $Re_L \approx 3.3 \times 10^5$ for the low-speed case and $Re_L \approx 8 \times 10^5$ for the high-speed case which results in a boundary layer thickness of about $\delta(x) \approx$ 30 mm and 25 mm, respectively, at the end of the plate. The plate leading edge is placed at about 100 mm above the bottom wall so that it certainly does not lie inside a wall boundary layer. But due to the small channel height, the influence of the sidewall and top wall BLs has to be considered in the numerical analysis. Another aspect which should be kept in mind is the vertical position of the TE (trailing edge) of the plate (distance b in Fig. 1b). It has to be ensured that the boundary layer of the top wall does not "collide" with the investigated boundary layer of the plate. As already described the boundarylayer grows along the plate, thus an important value is the boundary layer thickness $\delta(x_{TE})$ at the trailing edge of the plate. In Fig. 2b this value is illustrated for different free stream velocities u_∞. Also the values for the two test cases are marked in the figure. The graph shows that there is a maximal BL thickness (about $\delta(x_{TE}) \approx$ 30 mm) which can be reached for a given plate length under normal operating conditions.

The position of the trailing edge could not be chosen freely, since the length of the plate is fixed with 939 mm and the angle is set to 2° as discussed before. However, so the resulting position of the TE has sufficient distance towards the top wall.

---

[1] Computed with the plate length L and the thermophysical properties at the inlet.

(a) Along the plate

(b) At the plate trailing edge where v changes in Re

Fig. 2   Graph of the boundary layer thickness $\delta(x)$.

Also the displacement thickness δ^* is important which describes the shift of the free-stream streamlines away from the surface where the boundary layer develops. It gives the distance which a surface with a boundary layer would have to be moved in perpendicular direction to have the same flow rate compared to a case of a surface without a boundary layer [1]. The displacement thickness can be calculated for an incompressible fluid with

$$\delta^* = \int_0^\infty \left(1 - \frac{u(y)}{u_\infty}\right) dy \qquad (3)$$

where, u represents the local streamwise velocity, y the direction normal to the wall and u_∞ represents the free stream velocity. δ^* influences the velocity of the free-stream within a channel (like in the test setup) since it narrows down the effective free stream flow area.

The tests were performed for two different channel cross sections W × H: 500 × 200 mm (low speed case) and 200 × 200 mm (high speed case).

4. Turbulence and Dissipation Measurements

Downstream of the diffuser with guiding vanes (position A in Fig. 1b) the free stream turbulence intensity Tu together with the total pressure p_t is measured. These values are measured about $x = 220$ mm upstream of the leading edge of the plate and are used as boundary conditions for the simulation.

Close to the leading edge (position B) again the turbulence intensity Tu is measured to be able to approximate the turbulence length scale of the flow which is necessary for the computational setup.

Tu measurements were performed by means of a cylindrical single-sensor FRAPP (fast-response aerodynamic pressure probe). A miniaturized

piezo-resistive pressure sensor (Kulite XCE-062) is mounted inside the probe head, which has an outer diameter of 1.85 mm.

The probe aerodynamic accuracy was evaluated in a calibrated nozzle, giving an extended uncertainty equal to $\pm 0.5\%$ of the kinetic head for the pressure measurements and equal to $\pm 0.5°$ for the flow angle. In order to obtain the transfer function of the probe, a dynamic calibration was carried out in a low-pressure shock tube; after digital compensation the probe bandwidth reaches up to 80 kHz. Persico et al. [25] presented more details about the probe design and calibration.

In order to get the turbulence intensity Tu out of the measured signal it is necessary to remove all periodic components of the raw measured signal. In order to perform this reduction, the measured signal is FFT (fast fourier transformed) and the periodic components (like blade passing frequency and its harmonics) of the signal are "chopped" [16]. Only the non-periodic stochastic parts of the signal are modeled by a single-point turbulence model (like $k - \omega$ or $k - \epsilon$) [17]. This chopped signal is illustrated in Fig. 3, where the amplitude of the velocity fluctuations over the frequency is presented.

In this figure also the $-5/3$-line, known from the Kolmogorov-Obukhov [26-28] spectrum, can be observed. The spectrum shows, that the fluctuations fit the $-5/3$-line up to about 10 kHz. Above this

frequency it can be assumed that the fluctuations are due to white noise and cannot be considered as turbulence. Also low-frequency fluctuations (lower than 500 Hz) are assumed to have no contribution to the turbulence level. Thus, only the fluctuations between 500 Hz and 10 kHz have been taken into account for the calculation of the turbulence intensity.

The chopped and filtered spectrum was then processed with an inverse FFT to get a time signal again [16].

This time signal of the turbulent velocity fluctuations is then used to determine the turbulence intensity Tu according to Ref. [16]:

$$Tu = \frac{1}{\bar{u}} \cdot \sqrt{\frac{1}{N} \cdot \sum_{i=1}^{N} \hat{u}_i^{\,2}} \qquad (4)$$

where, $\bar{u}$ represents the mean velocity and $\hat{u}_i$ represents the velocity fluctuations.

The turbulence intensity is a crucial and important inlet parameter for the simulation. Beside Tu another factor, the turbulence length scale l, needs to be defined at the inlet to determine the turbulence dissipation rate. Unfortunately the length scale is not often measured since it is more a descriptive quantity for explaining the dissipation. The idea of a mixing length was introduced by Prandtl [29] in 1925 describing it as "only a rough approximation" [30]. Prandtl made a correlation between the turbulence shear stress τ_t and the velocity
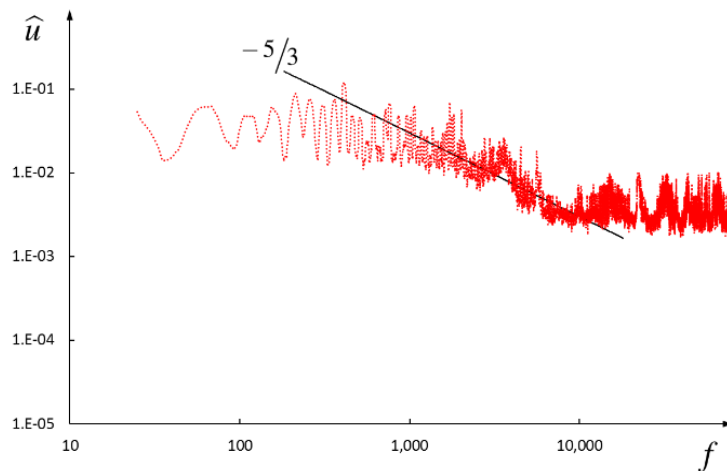

Fig. 3   Moving average of the chopped velocity fluctuations over the frequency.

gradient in a viscous layer. Therefore he introduced the mixing length l_m which describes the mean free distance between two eddies [1].

Although it is only a model for understanding the process of dissipation, it is still used in modern CFD codes. Since it is only a theoretical quantity, it is neglected in most measurements, and in most publications no focus on the length scale or dissipation is laid on.

In the following different definitions of the turbulence length scale are given. Several overviews have been published in the last years like Refs. [16, 17, 31, 32] and in the following the main outcomes will be discussed.

To use the above discussed mixing length in CFD calculations, a correlation between the mixing length l_m and the dissipation rate ϵ is necessary. This correlation is known as *Prandtl-Kolmogorov*-equation [1].

$$\epsilon = C_\mu^{3/4} \cdot \frac{k^{3/2}}{l_m} \tag{5}$$

where, k represents the turbulence kinetic energy and $C_\mu^{3/4}$ represents an empirical constant (usually ≈ 0.09) which is specified by the used turbulence model [33]. This correlation is used by codes like Fluent®, LINARS and several other codes. For estimating this mixing length the Fluent® modeling guide recommends l_m with

$$l_m = 0.07 \cdot H \tag{6}$$

where, H represents the hydraulic/characteristic diameter.

Other CFD codes (like CFX®) use a length scale defined as

$$l = \frac{k^{3/2}}{\epsilon} \tag{7}$$

This definition of a length scale is often called *pseudo-integral scale* as suggested by Gamard and George [31].

The two given definitions above (Eqs. (5) and (7)) represent a relation between the turbulence kinetic

energy and dissipation, but the problem is that l and l_m are not directly measurable.

Since the length scale is used to define the turbulent dissipation rate ϵ it is obvious to measure this flow variable directly. Unfortunately this is almost impossible, since it would be necessary to measure down to very small spatial resolutions which cannot be resolved by probes [17].

A length which is measurable is the so-called (physical) integral length scale L which is defined as Ref. [16].

$$L = \bar{u} \cdot \int_0^k ACF(\tau)d\tau \tag{8}$$

where, $ACF(\tau)$ represents the ACF (autocorrelation function) of the turbulent velocity signal. In order to determine L the chopped FFT spectrum which was used within the signal processing for obtaining the turbulence intensity Tu is multiplied by its conjugated complex part and then transformed back with an inverse-FFT. The time signal obtained this way is then autocorrelated [16].

The idea behind the integral length scale L is that it describes the time a turbulence fluctuation needs to dissipate its energy. This time then is converted with the mean velocity $\bar{u}$ to a physical length.

The problem evolving from these definitions is that the idea of a turbulence length as parameter for the dissipation is more or less rough and dissatisfactory. So far, three different length scales have been defined:

(1) The physical integral scale L which is measurable;

(2) The pseudo-integral scale l which is used e.g. by CFX®;

Table 1 Measured and computed values of Tu and ϵ at the inlet (Pos. A) and within the channel (Pos. B).

Turbulence Tu	
Position A:	$Tu = 9.24\%$
Position B:	$Tu = 9.0\%$
Dissipation ϵ	
Linear develop:	$\epsilon_L = 14.686 \;\; m^2/s^3$
Exponent develop:	$\epsilon_E = 15.2485 \;\; m^2/s^3$

(3) The mixing-length idea l_m which is used e.g. by Fluent[®];

While l and l_m have a clear relationship ($\frac{l_m}{l} = C_\mu^{3/4}$), the relation between l or l_m and L is not clear and depends on the investigated flow.

In order to get a boundary condition for the dissipation rate ϵ another approach will be discussed within this work.

As discussed before, the fluctuations are measured at two positions: At the inlet of the test section and within the channel (positions A and B in Fig. 1b). At these positions the turbulence intensity is determined. The Tu-values are given in Table 1.

Using the measured turbulence values at the two different positions the dissipation rate ϵ can be determined directly. Starting from the transport equation for k with the assumption of a non-accelerating flow with a isotropic turbulence the equation for the change of the turbulence kinetic energy [32]

$$\frac{dk}{dt} = P - \epsilon \qquad (9)$$

can be used. For a steady flow without turbulence production between the two measurement positions following approximation can be used:

$$\bar{u} \cdot \frac{dk}{dt} = -\epsilon \qquad (10)$$

Since the used evaluation system gives Tu the turbulent kinetic energy is obtained by using Eq. (11)

$$k = \frac{3}{2} \cdot \left[\frac{Tu[\%]}{100} \cdot \bar{u} \right]^2 \qquad (11)$$

at both measurement positions. Since the distance between these two measurement positions is known as well as the kinetic energy k at these positions, ϵ can be estimated by using Eq. (10). In a first approach a linear decrease of the turbulence kinetic energy between the two positions is assumed, thus ϵ is constant.

Another approach is to assume an exponential decrease of k between the two measurement positions according to

$$k = k_0 \cdot e^{-a \cdot x} \qquad (12)$$

where, a can be seen as decay exponent and describes how the turbulence dissipates within the flow. Eq. (12) can be used to calculate k at any position based on a starting value k_0.

Since $k(x)$, k_0 and the distance are known in our test case, the decay exponent a for the wind tunnel can be computed and thus the gradient of k at the inlet $[dk/dx]_{Inlet}$. Inserting this into Eq. (10) leads to the dissipation rate ϵ at the inlet which can be calculated with

$$\epsilon = -\bar{u} \cdot \left[\frac{dk}{dx} \right]_{Inlet} \qquad (13)$$

The results of these evaluations are given in Table 1 where ϵ_L represents the solution with a linear and ϵ_E with an exponential decrease of k, respectively. Due to the small change of the measured turbulence intensity the difference between the two ϵ-values is small.

To sum up, five different options for the determination of the turbulence dissipation have been showed: Three length scales (physical integral length scale L, pseudo-integral scale l and mixing length l_m) and two ϵ-values.

In Table 2 the different length scales are listed: L represents the measured value, l_m represents the mixing-length used by LINARS and Fluent[®] (l_m^* is the mixing-length as recommend by the Fluent modeling guide (see Eq. (6))) and l represents the pseudo-integral length scale used by CFX[®]. The suffixes L and E represent the dissipation assumption whether it is linear or exponential.

Table 2 clearly shows that the differences between the different length scales are remarkable. To see the influence of the different length scales, simulation results computed with Fluent[®] and CFX[®] are given in Fig. 4. The graph shows the development of the turbulence intensity Tu from the inlet to the measurement position B.

The measured physical integral length scale $L =$

Table 2   Different length scale in meters.

Measurement	$L = 0.18158\ m$
Fluent, modeling guide value	$l_m^* = 0.014\ m$
Fluent, from measured ϵ_L	$l_{m,L} = 0.0575\ m$
Fluent, from measured ϵ_E	$l_{m,E} = 0.0554\ m$
CFX, from measured ϵ_L	$l_L = 0.35\ m$
CFX, from measured ϵ_E	$l_E = 0.337\ m$

0.18158 m shows a too weak dissipation, while the recommended mixing length $l_m^* = 0.014$ m shows a too high dissipation. Both length scales do not fit with the measured decrease of turbulence intensity.

The pseudo-integral scales l and mixing lengths l_m computed from the measured ϵ-values show nearly the same decrease of turbulence intensity as the measured one. It is also observable, that the differences between the assumed linear and exponential turbulence decrease are not high, but the exponential decrease fits slightly better to the measured results.

Both CFX® simulations show a too high turbulence intensity at the inlet, although the same value of $Tu = 9.24\%$ has been specified. However, CFX® computes the same decrease of Tu compared to Fluent® and the measurement.

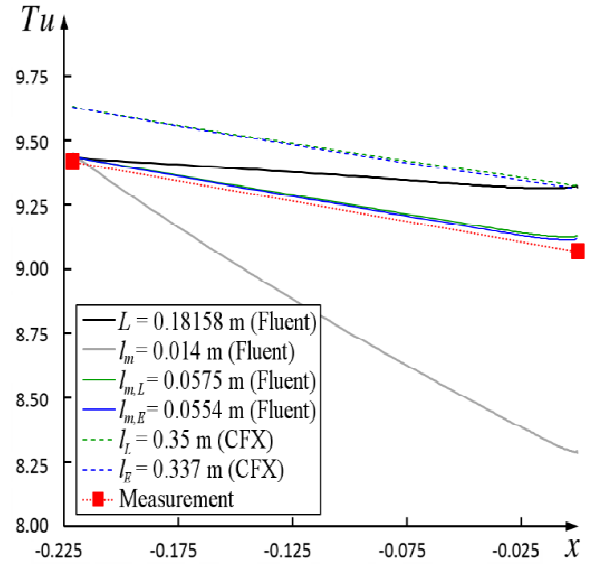For the sake of completeness it has to be mentioned that LINARS (also using the mixing-length approach) computes the same development as Fluent®, but is not illustrated in Fig. 4 due to clarity of the chart.

5. Transition Measurements

In this section the measurement and visualization of the transition process at the flat plate are discussed.

Along the flat plate several static pressure tappings are embedded into the plate. The diameter of the tappings is 0.5 mm. These measurement positions are used for Preston-tube measurements.

A Preston tube is traversed all over the plate in streamwise direction in order to locate the transition region. The probe consists of a pitot tube with an inner diameter of 0.5 mm. The Preston tube allows to measure the dynamic pressure close to the wall. This pressure can then be used to calculate the non-dimensional dynamic pressure according to Ref. [35]:

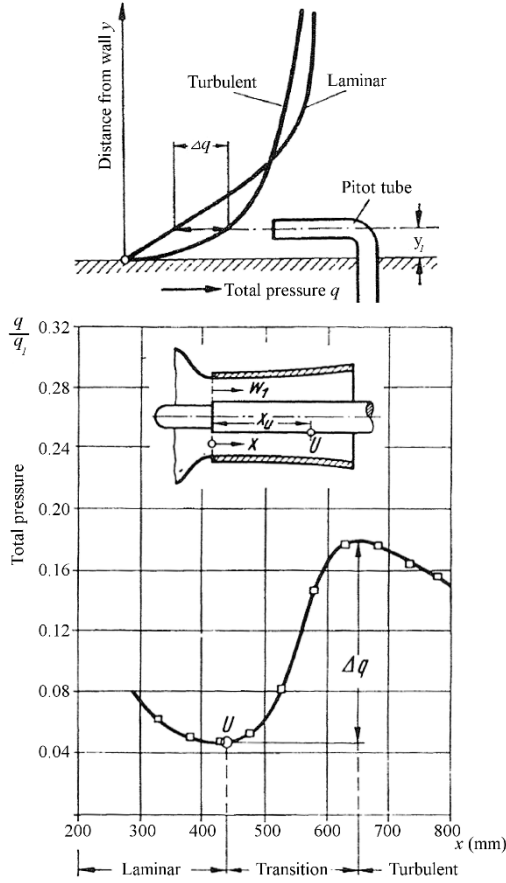**Fig. 4   Simulation results with different length scales.**

$$\frac{q_{probe}}{q_\infty} = \frac{p_{t,probe}(x) - p(x)}{p_{t,\infty} - p(x)} \qquad (14)$$

where, $p_{t,probe}(x)$ and $p(x)$ represent the total and static pressure acquired by the probe and the tappings, and $p_{t,\infty}$ represents the free-stream total pressure. The result gives an indication of the shape of the velocity profile close to the wall which is then characteristic for the state of the boundary layer. Fig. 5 explains this idea: The upper sketch shows the different velocity profiles of the laminar and turbulent boundary layer. The higher velocity close to the wall of the turbulent boundary layer is due to the fact that more energy can be transported normal to the streamwise direction towards the wall because of its turbulent state [34].

The lower sketch in Fig. 5 shows the streamwise distribution of the non-dimensional dynamic pressure q_{probe}/q_∞ (here q/q_1) and gives an example how the value increases when transition occurs.

However, the probe size has to be kept in mind, since the measured result can only be valid as long as the thickness of the boundary layer is at least twice the distance of the probe from the wall (y_1 in Fig. 5).
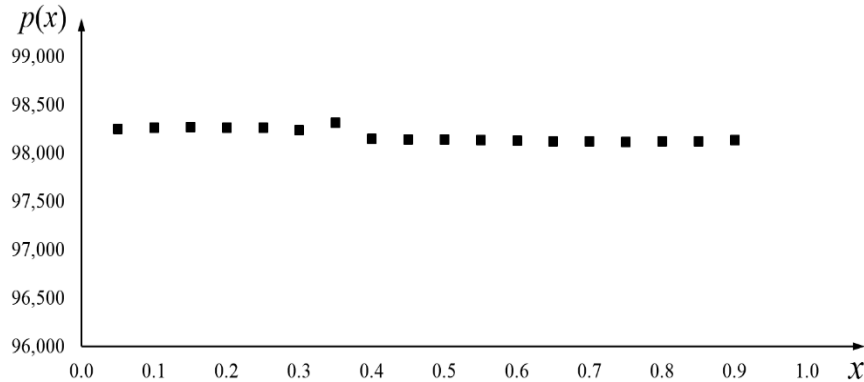
As already described, two measurements were performed for two different inlet velocities: $u_{\infty,mean} = 5.3$ m/s and $u_{\infty,mean} = 13.2$ m/s. The turbulence intensity together with the total pressure have been

Fig. 5   Explanation of the Preston tube measurement theory.

measured at the inlet plane and the turbulence additionally close to the leading edge of the plate. The values at the inlet plane together with the static pressure at the outlet are used as boundary conditions for the simulations described later.

In Fig. 6 the static pressure along the flat plate is illustrated. The laminar and the turbulent zone are separated by a small peak within the static pressure

which is caused by laminar-to-turbulent transition.

The measured q_{probe}/q_∞ values of both test runs are given in Fig. 7. No transition can be observed for the low speed test case. This also agrees with the above mentioned critical Reynolds number $Re_{x,crit}$ as onset criterion. According to this, transition would start at about the position of the trailing edge of the plate.

The high speed measurements clearly show the start of transition (rise of q_{probe}/q_∞) at about 350-400 mm. This again agrees with the assumed onset criterion stated above.

In order to verify the measured transition location, the change of the boundary layer is visualized with the help of a thermographic camera. Since the heat transfer coefficient depends highly on the state of the boundary layer, the surface temperature of a heated plate changes when the boundary layer transitions from laminar to turbulent. The difference in heat transfer can be described by the heat transfer coefficient α which can be calculated with the Nusselt-number defined as

$$Nu_x = \frac{\alpha \cdot x}{\lambda_L} \tag{15}$$

where, λ_L represents the thermal conductivity. Nu_x changes with the state of the boundary layer according to Ref. [36]:

$$Nu_x = 0.332 \cdot Re_x^{0.5} \cdot Pr_x^{0.5} \quad \text{laminar} \tag{16}$$
$$Nu_x = 0.0296 \cdot Re_x^{0.8} \cdot Pr_x^{1/3} \quad \text{turbulent} \tag{17}$$

where, Pr represents the Prandtl number. The correlation between Re_x and Nu_x and thus α isillustrated in Fig. 8 (Pr = 0.71486 for air at 20 °C, 1 bar). In this graph again the critical Reynolds number

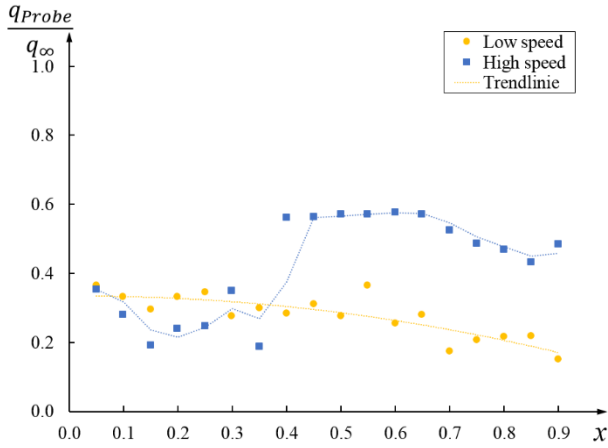**Fig. 6   Static pressure along the flat plate for the high speed test case.**

Fig. 7 q_{probe}/q_∞ measurements along the flat plate.

of 3×10^5 is assumed as transition onset criterion.

For the visualization a FLIR® SC620 thermographic camera was used which has a sensitivity < 40 mK at 30 °C. The camera was placed above an optical access at the top of the channel (illustrated in Fig. 1b) and recorded about 100 mm of the plate length.

On the flat plate a heating foil was glued with a constant heating input. The optical access was placed in such a way, that it is situated above the expected transition zone.

The result of the visualization is given in Fig. 9. The picture shows that the temperature of the heating foil drops at about 410 mm plate length. This most likely indicates a transitional zone and agrees well with the results of the Preston probe measurements.

6. Transition Simulation

Both measurement techniques showed that transition

occurs at approximately 400 mm plate length. In the following numerical results are compared with the measurements to see how the transition model can predict the measured transition zone.

All inlet conditions are taken from the measurement. For the length scale $l_{m,L} = 0.0575\ m$ for Fluent® and LINARS and $l_L = 0.35\ m$ for CFX® are used which have been computed from the measured dissipation rate ϵ.

Fig. 10a shows the skin friction coefficient c_f at the plate for all three simulations. c_f is defined as

$$c_f = \frac{\tau_W}{\frac{1}{2} \cdot \rho \cdot u_\infty^2} \tag{18}$$

where, τ_W is the wall shear stress and u_∞ is the free stream velocity. All three codes used the $\gamma - Re_\Theta$-model and Fluent® additionally the $k - k_L - \omega$-model. All three codes failed in predicting the measured transition zone with the $\gamma - Re_\Theta$ model. The skin friction values show a fully turbulent boundary layer along the plate surface.

On the other hand, the $k - k_L - \omega$ turbulence model predicted successfully a transitional zone although it starts more upstream compared to the measured transition location.

A possible reason for not predicting transition with the $\gamma - Re_\Theta$-model is observable in Fig. 10b which shows the skin friction development along the flat plate for different turbulence intensities Tu computed with Fluent®. The chart shows, that for decreasing inlet
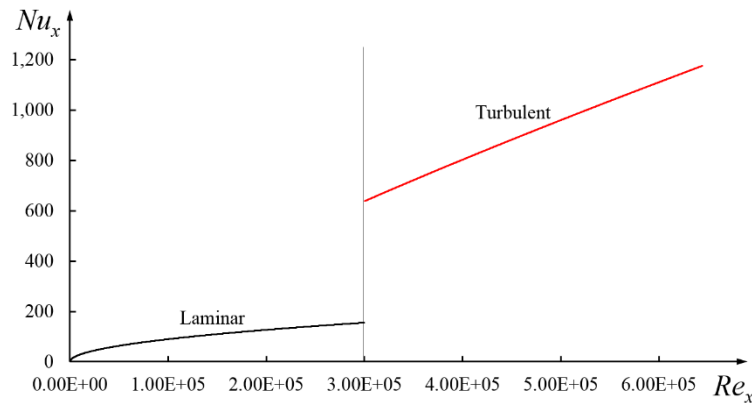

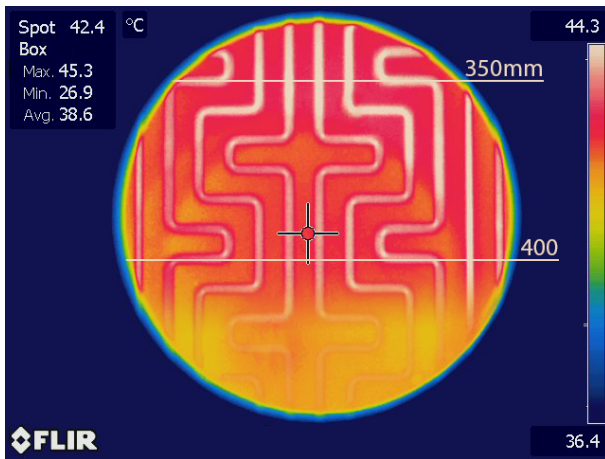**Fig. 8 Nusselt number over Reynolds number for laminar and turbulent boundary layer.**

Fig. 9   Recording of the thermographic camera.

(a) Comparing the three codes

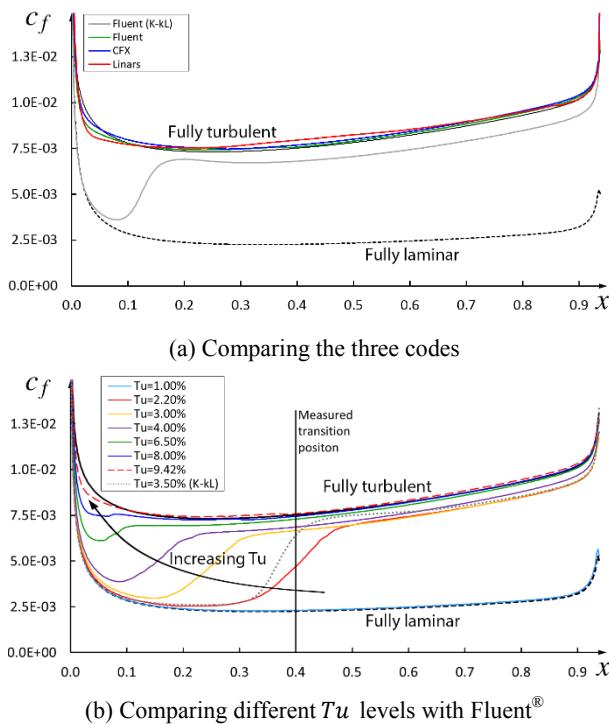(b) Comparing different Tu levels with Fluent®

Fig. 10   Computed development of skin friction coefficient c_f along the flat plate.

turbulence intensity Tu transition is predicted. With an inlet turbulence intensity of about $Tu = 2.2\%$ the simulation shows a similar transition position as the measurements. At $Tu = 1\%$ no transition is observable anymore since the boundary layer stays laminar along the whole plate. It seems that for the high inlet turbulence the $\gamma - Re_\Theta$ transition model is not able to predict a laminar flow at the leading edge of the plate; thus no transition can be observed.

In Fig. 10b, also the $k - k_L - \omega$ model result is given for a lower inlet turbulence intensity. For $Tu = 3.5\%$ this model predicts a similar onset of the transition zone as the measurements. Compared to the $\gamma - Re_\Theta$-model result, the transitional zone is also smaller, which agrees better with the measurements, since the increase of q_{probe}/q_∞ spans only the distance between two measurement positions (see Fig. 7).

Both models show a different behavior when varying the turbulence intensity, but both react sensibly to the boundary condition.

7. Summary and Conclusions

In the present work the transition on a flat plate has been investigated. The measurements and simulations performed in the scope of this work are intended for a better understanding of transition prediction, both experimentally and numerically.

First, the paper describes the setup of a test bench. Therefore several important considerations are described which should be followed when designing such a test facility.

One major outcome of the study is that the turbulence inlet boundary conditions of the numerical simulations have a high impact on the result of the simulation, especially when it comes to transition. The investigation also showed that there are differences in the definition of the turbulence length scales and the needed length scale for the simulation cannot be measured directly. A general correlation between the measured integral length scale and the pseudo-length scale used by CFD would be helpful, but this needs more experimental data.

Two different techniques to measure and visualize transition have been tested successfully: Preston tube measurements and visualization with a thermographic camera. Regarding the computational results, the $\gamma - Re_\Theta$-model was not able to predict the transition process of this test case as observed in the measurements. On the other hand the $k - k_L - \omega$ turbulence model could predict transition but at a more upstream position.

Further numerical studies are necessary to understand the deficiencies of these models.

Further experimental and numerical studies are planned and should help to better understand the complex mechanism of transition. The result will form the basis for further studies on the mechanism of relaminarization.

Acknowledgement

References

[1] Schlichting, H., and Gersten, K. 2006. *Grenzschicht-Theorie (Boundary-Layer Theory)*. Springer-Verlag Berlin Heidelberg.

[2] Mayle, R. E. 1991. "The Role of Laminar-Turbulent Transition in Gas Turbine Engines." *Journal of Turbomachinery* 113 (October): 509-37.

[3] Yip, L. P., Vijgen, P., Hardin, J. D., and Van Dam, C. P. 1993. "In-flight Pressure Distributions and Skin-Friction Measurements on a Subsonic Transport High-Lift Wing Section." Presented at AGARD, High-Lift System Aerodynamics.

[4] Oyewola, O., Djenidi, L., and Antonia, R. A. 2003. "Combined Influence of the Reynolds Number and Localised Wall Suction on a Turbulent Boundary Layer." *Experiments in Fluids* 35 (July): 199-206.

[5] Oyewola, O. 2006. "LDV Measurements in a Pertubed Turbulent Boundary Layer." *Journal of Applied Science* 6 (14): 2952-5.

[6] Widmann, A., Duchmann, A., Kurz, A., Grundmann, S., and Tropea, C. 2012. "Measuring Tollmien-Schlichting Waves Using Phase-Averaged Particle Image Velocimetry." *Experiments in Fluids* 53 (3): 707-15.

[7] Mukund, R., Narasimha, R., Viswanath, P. R., and Crouch, J. D. 2012. "Multiple Laminar-Turbulent Transition Cycles Around a Swept Leading Edge." *Experiments in Fluids* 53 (6): 1915-27.

[8] Walters, K., and Cokljat, D. 2008. "A Three-Equation Eddy-Viscosity Model for Reynolds-Averaged Navier-Stokes Simulations of Transitional Flows." *Journal of Fluids Engineering* 130 (12): (121401) 1-14.

[9] Menter, F. R., Langtry, R. B., Likki, S. R., Suzen, Y. B., Huang, P. G., and Völker, S. 2006. "A Correlation Based Transition Model Using Local Variables Part 1: Model Formulation." *Journal of Turbomachinery* 128 (3): 413-22.

[10] Langtry, R. B. 2006. "A Correlation-Based Transition Model Using Local Variables for Unstructured Parallelized CFD Codes." Ph.D. thesis, University Stuttgart.

[11] Elsner, W., Piotrowski, W., and Drobniak, S. 2008. "Transition Prediction on Turbine Blade Profile with Intermittency Transport Equation." *Journal of Turbomachinery* 132 (1): 11-20.

[12] Langtry, R. B., and Menter, F. R. 2009. "Correlation Based Transition Modeling for Unstructured Parallelized Computational Fluid Dynamics Codes." *American Institute of Aeronautics and Astronautics Journal* 47 (12): 2894-906.

[13] Sorensen, N. N. 2009. "CFD Modeling of Laminar-Turbulent Transition for Airfoil and Rotors Using the $\gamma-Re_\Theta$ Model." *Wind Energy* 12 (8): 715-33.

[14] Malan, P., Suluksna, K., and Juntasaro, E. 2009. "Calibrating the $\gamma-Re_\Theta$ Transition Model for Commercial CFD." In *Proceedings of the 47th AIAA Aerospace Sciences Meeting Including the New Horizons Forum and Aerospace Exposition,* 1-20.

[15] Kelterer, M. E., Pecnik, R., and Sanz, W. 2010. "Computation of Laminar-Turbulent Transition in Turbomachinery Using the Correlation Based $\gamma-Re_\Theta$ Transition Model." In *Proceedings of the ASME Turbo Expo,* 613-22.

[16] Camp, T. R., and Shin, H. W. 1995. "Turbulence Intensity and Length Scale Measurements in Multistage Compressors." *Journal of Turbomachinery* 117 (January): 38-46.

[17] Axelsson, L.-U., and George, W. 2008. "Spectral Analysis of the Flow in an Intermediate Turbine Duct." In *Proceedings of the ASME Turbo Expo,* 1419-26.

[18] Axelsson, L.-U. 2009. "Experimental Investigation of the Flow Field in an Aggressive Intermediate Turbine Duct." Ph.D. thesis, Chalmers University of Technology.

[19] Craft, T. J. 2011. *Turbulence Length Scales and Spectra*. Lecture Notes for Advanced Turbulence modeling, The University of Manchester.

[20] ANSYS. 2012. *Ansys CFX-Solver Modeling Guide*. Release 14.5. ANSYS Inc.

[21] Pecnik, R., Pieringer, P., and Sanz, W. 2005. "Numerical Investigation of the Secondary Flow of a Transonic Turbine Stage Using Various Turbulence Closures." In *Proceedings of the ASME Turbo Expo,* 1185-93.

[22] Roe, P. L. 1997. "Approximate Riemann Solver, Parameter Vectors, and Differencing Scheme." *Journal of Computational Physics* 135 (2): 250-8.

[23] Menter, F. R. 1994. "Two-Equation Eddy-Viscosity Turbulence Models for Engineering Applications." *American Institute of Aeronautics and Astronautics Journal* 32 (8): 1598-605.

[24] Coupland, J. 1990. "Flat Plate Transitional Boundary Layers." ERCOFTAC "Classic Collection" Database. Accessed March 15, 2016. http://cfd.mace.manchester.ac.uk/cgi-bin/cfddb/ezdb.cgi?ercdb+search+retrieve+&&&SemiCFlow1g=Yes%%%%dm=Line.

[25] Persico, G., Gaetani, P., and Guardone, A. 2005. "Design and Analysis of New Concept Fast-Response Pressure Probes." *Measurement Science and Technology* 16 (9): 1741-50.

[26] Kolmogorov, A. N. 1991. "The Local Structure of Turbulence in Incompressible Viscous Fluid for Very Large Reynolds Numbers." *Proceedings: Mathematical and Physical Sciences* 434 (1890): 9-13.

[27] Kolmogorov, A. N. 1991. "Dissipation of Energy in a Locally Isotropic Turbulence." *Proceedings: Mathematical and Physical Sciences* 434 (1890): 15-17.

[28] Obukhov, A. M. 1941. "On the Distribution of Energy in the Spectrum of Turbulent Flow." *Doklady Akademii Nauk SSSR* 32 (1): 22-4.

[29] Prandtl, L. 1925. "Bericht Über Untersuchungen Ausgebildeter Turbulenz." *Zeitschrift Für Angewandte Mathematik und Mechanik* 5 (2): 136-9.

[30] Bradshaw, P. 1974. "Possible Origin of Prandtl's Mixing-Length Theory." *Nature* 249 (6): 135-6.

[31] Gamard, S., and George, W. K. 2000. "Reynolds Number Dependence of Energy Spectra in the Overlap Region of Isotropic Turbulence." *Flow, Turbulence and Combustion* 63 (1-4): 443-77.

[32] Pope, S. B. 2000. *Turbulent Flows*. Cambridge: Cambridge University Press.

[33] ANSYS. 2015. "Using Flow Boundary Conditions." In *Ansys Fluent Documentation*, Release 16.0. ANSYS Inc.

[34] Schlichting, H. 1965. *Grenzschicht-Theorie (Boundary-Layer-Theory)*. Verlag G. Braun, Karlsruhe.

[35] Händel, D., Rockstroh, U., and Niehuis, R. 2014. "Experimental Investigation of Transition and Separation Phenomena on an Inlet Guide Vane with Symmetric Profile at Different Stagger Angles and Reynolds Numbers." In *Proceedings of the 15th International Symposiumon Transport Phenomena and Dynamics of Rotating Machinery,* 1-9.

[36] Polifke, W., and Kopitz, J. 2005. "Wärmeübertragung." *Heat Transfer, Pearson Education, München*.